Turk J Elec Engin, VOL.10, NO.2 2002, © TÜBİTAK

2D Complex Point Source Radiation Problem II. Complex Beams

M. J. GONZÁLEZ MORALES, E. GAGO-RIBAS
Dpto. Teoría de la Señal y Comunicaciones e I.T., Universidad de Valladolid-SPAIN
e-mail: emigag@gbien.tel.uva.es
e-mail: chus@gbien.tel.uva.es

Abstract

The complex point source analytic continuation, and the analysis into the spaces of complex distances, angles, and other related magnitudes, may be applied to describe a wide variety of 2D wave propagation problems. This step will be essential in order to establish a complete **complex** *methodology which may be applied to obtain general descriptions of more practical problems involving the scattering of waves under some kind of field incidence. A particular application of the methodology presented in Part I will be used in Part II. The specific problem under analysis in these papers will be the general complex beam solution obtained from the analytical continuation of the real space Green's function, solution of the 2D Helmholtz equation in free space, into the space of complex coordinates. As obtained in Part I, the general complex beam solution turns out a great variety of solutions, each one associated to a specific practical approximation. The complete set of solutions for this particular problem, already presented in Part I, will be analyzed here in detail. The initial representation of the problem in terms of different regions associated to each solution (obtained by parameterizing each approximation into the complex distances and complex angles spaces), will be used here to describe the behavior (amplitude profile, phase fronts, energy phase paths, etc.) for each solution, such as non homogeneous cylindrical waves or pseudo-Gaussian beams, elliptical-phase non homogeneous cylindrical waves, Gaussian beams, etc. The complex representation of important magnitudes such as phase and energy paths will be analyzed here by using some of the mappings presented in Part I. This kind of interpretations will be essential when trying to understand complex rays, complex image sources or complex caustics in later scattering problems. The methodology, described first in Part I and completed now in Part II, should conform a general basis to study other wave propagation problems described in terms of complex source coordinates.*

Key Words: *complex source, radiation, Gaussian beam, paraxial condition, propagation*

1. Introduction

It is known, as it was shown in **Part I**, that the Green's function for a complex point source radiation problem is,

$$G_f(\vec{r},\vec{\mathbf{r}}_\mathbf{s}) = \frac{i}{4}H_0^{(1)}(k_0|\vec{r}-\vec{\mathbf{r}}_\mathbf{s}|) = \frac{i}{4}H_0^{(1)}(k_0\mathbf{R}_\mathbf{s}) \tag{1}$$

with,

$$|\vec{r}-\vec{\mathbf{r}}_\mathbf{s}| = k_0\mathbf{R}_\mathbf{s} = \sqrt{(x-\mathbf{x}_\mathbf{s})^2+(z-\mathbf{z}_\mathbf{s})^2}. \tag{2}$$

This is only valid provided that the field satisfies physical conditions, such as the radiation condition at infinity, [1]. In connection with this, the analysis developed in **Part I** revealed the constrains, [2] which must be imposed to the complex argument of the Green's function. *Even when the replacement of* $\vec{r}_s$ *by* $\vec{\mathbf{r}}_\mathbf{s}$ *yields a valid field solution, the interpretation of these solutions is not elucidated by the simple process of the analytic continuation*, [3]. This property of the complex source point field has important consequences. It implies that *any field solution for which the incident field is a cylindrical wave, can be converted into a solution for an incident beam*, [3].

In the present paper we will focus in the Green's function analysis and its approximations, provided that any component of the fields $\vec{E}$ and $\vec{H}$ may be represented in terms of the Green's function in the complex-point source radiation problem. The classification of the solutions was given in Figure 2, **Part I**.

As already described in **Part I**, the analysis presented here constitutes a specific example of the application of the complex analysis for a particular wave propagation problem. As shown in [2], other types of wave propagation phenomena, such as *evanescent plane waves* and *surface waves*, may be obtained and described in terms of the complex parameterization presented in **Part I**. Based on these parameterizations, the procedure used to analyze these kind of wave solutions follows a similar methodology to that described in the present paper.

2. Complex Beams

The Green's function for the exact solution, named *Complex Beams* (CB) was written in (1). As long as this is the exact solution and the values may only be obtained numerically, the unique analysis here is how to trace the shape of the solution. The amplitude and phase of the Hankel function of zero order and first kind $H_0^{(1)}(k_0\mathbf{R_s})$ are represented in Figure 1 in the half plane $\Re\{k_0\mathbf{R_s}\} \geq 0$ in terms of the real and imaginary parts of its complex argument[1]. The restriction $\Re\{k_0\mathbf{R_s}\} \geq 0$ will be imposed in order to carry out the radiation condition at infinity. The amplitude and phase of the same function are represented in Figure 2 in terms of the real propagation coordinates (ξ, η). Some considerations about how to obtain the values of the exact solution may be found in Appendix I.

Although the exact Green's function solution is not the more efficient from a practical point of view, it constitutes a reference standard against which other formulations and approximations may be qualitatively and quantitatively compared, [4]. Some of the mappings studied in Part I are based on its particular complex behavior. As it will be seen in next sections, the ranges of validity and domains of definition appearing from the different approximations considered will be parameterized in terms of quantitative non-dimensional estimations (ρ_{CRC}, ρ_{PC} and ρ_{HN}). Some of the complex boundary limits arising from these parameterizations constitute some of the mappings already generalized and studied in **Part I**.

3. Non Homogeneous Cylindrical Waves

3.1. Complex radiation condition

The Hankel function of zero order and first kind may be asymptotically evaluated for large values of the argument. Under this condition the field generated by a 2D complex point source will have a expression similar to a cylindrical wave, but with a complex phase due to the complex spatial coordinates in (2),

[1] Calling $\mathbf{R_s} = u + iv$, the real and imaginary parts of its complex argument are (k_0u, k_0v).

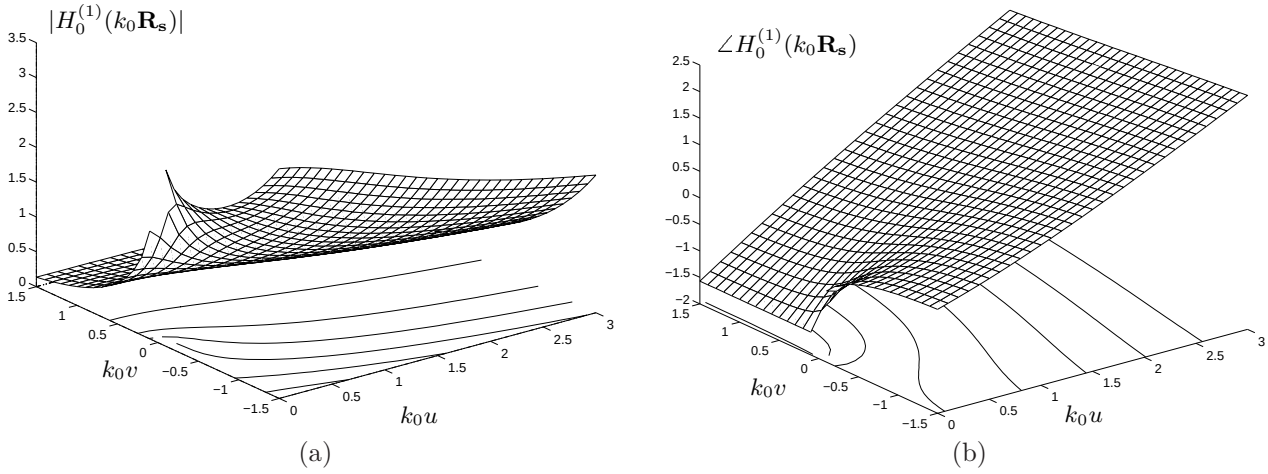

Figure 1. Hankel function of zero order and first kind $H_0^{(1)}(k_0\mathbf{R_s})$ in the half plane $\Re\{k_0\mathbf{R_s}\} > 0$. (a) Amplitude: $|H_0^{(1)}(k_0\mathbf{R_s})|$, and (b) phase: $\angle H_0^{(1)}(k_0\mathbf{R_s})$. The results were obtained with $k_0 = 1$, $\Re\{k_0\mathbf{R_s}\} \in (0, 3)$ and $\Im\{k_0\mathbf{R_s}\} \in (-2, 2)$.

leading to a *Non Homogeneous Cylindrical Wave* (NHCW). This asymptotic condition will be called *Complex Radiation Condition* (*CRC*) and may be defined as,

$$k_0|\mathbf{R_s}| \geq 1. \tag{3}$$

The *CRC* may be parameterized in terms circumferences of radius ρ_{CRC} through the analysis of the following condition,

$$k_0|\mathbf{R_s}| = \rho_{CRC}, \quad \rho_{CRC} \geq 1. \tag{4}$$

This is a *High Frequency-Far Field Condition* (*HF-FFC*) because involves a combination of $k_0 \gg 1$, which is related to high frequency, and/or $|\mathbf{R_s}| \gg 1$, which is a complex condition related to to the real far field condition.

Using the asymptotic expression for large arguments in [5],

$$H_0^{(1)}(\mathbf{z}) \sim \sqrt{\frac{2}{\pi\mathbf{z}}} e^{-i\frac{\pi}{4}} e^{i\mathbf{z}}, \qquad |\mathbf{z}| \to \infty, \tag{5}$$

and applying this result to (1), the Green's function may be written as:

$$G_f(\vec{r}, \vec{\mathbf{r}}_\mathbf{s}) \sim \frac{e^{i\frac{\pi}{4}}}{2\sqrt{2\pi}} \frac{e^{ik_0|\vec{r}-\vec{\mathbf{r}}_\mathbf{s}|}}{\sqrt{k_0|\vec{r}-\vec{\mathbf{r}}_\mathbf{s}|}}, \tag{6}$$

or,

$$G_f(k_0\mathbf{R_s}) \sim \frac{e^{i\frac{\pi}{4}}}{2\sqrt{2\pi}} \frac{e^{ik_0\mathbf{R_s}}}{\sqrt{k_0\mathbf{R_s}}}. \tag{7}$$

In a similar way as we did in Section 2, we could show the shape of the asymptotic approximation of the Hankel function given by (7), only in $\Re\{k_0\mathbf{R_s}\} \geq 0$ for the same reason as in previous section.

The error defined as the difference between the Hankel function and its asymptotic approximation is shown in Figure 3. There is an exponential decrease with increasing values of $k_0|\mathbf{R_s}|$. A similar result is obtained for the error in the argument.

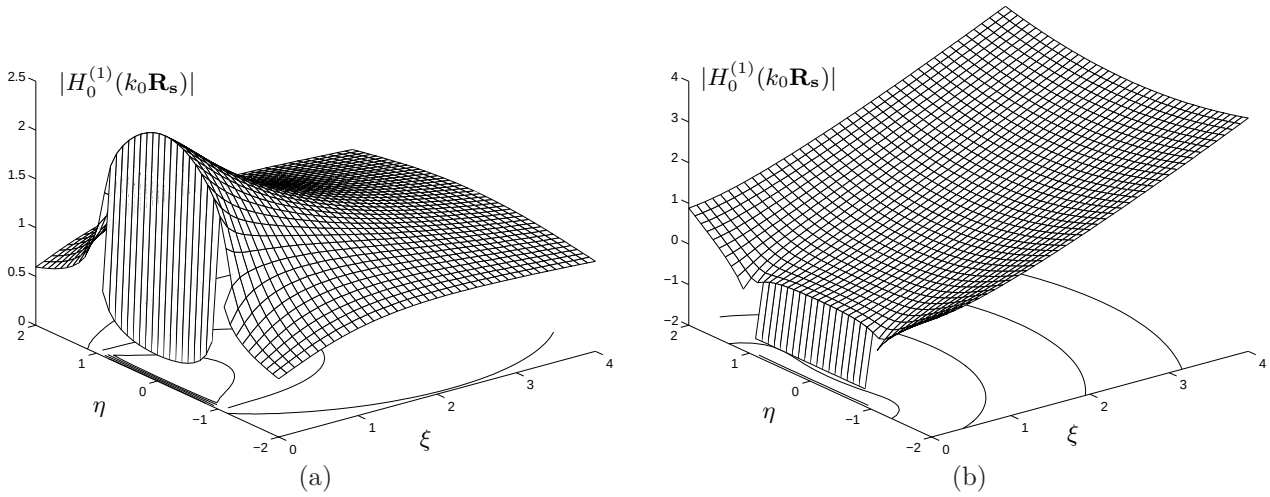

Figure 2. Complex beam in terms of the RPS. The results were obtained with $k_0 = 1$, $b = 1$, $\xi \in (0, 4)$ and $\eta \in (-2, 2)$. (a) Amplitude: $|H_0^{(1)}(k_0\mathbf{R_s})|$, and (b) phase: $\angle H_0^{(1)}(k_0\mathbf{R_s})$.

Let us define the error when (1) is approximated by (7). The relative error in the amplitude is define as,

$$\varepsilon_a = \frac{\left| H_0^{(1)}(k_0\mathbf{R_s}) - \sqrt{\frac{2}{\pi}} e^{i\frac{\pi}{4}} \frac{e^{k_0\mathbf{R_s}}}{\sqrt{k_0\mathbf{R_s}}} \right|}{|H_0^{(1)}(k_0\mathbf{R_s})|}, \tag{8}$$

and the error in the phase as,

$$\varepsilon_p = \angle \left\{ H_0^{(1)}(k_0\mathbf{R_s}) - \sqrt{\frac{2}{\pi}} e^{i\frac{\pi}{4}} \frac{e^{k_0\mathbf{R_s}}}{\sqrt{k_0\mathbf{R_s}}} \right\} \cdot \frac{180}{\pi}. \tag{9}$$

Figure 4 shows the curves with constant ε_a and ε_p. The curves with constant relative error in the absolute value may be approximated by semi-circumferences centered at the origin of coordinates. As larger is the radius of these circumferences, smaller is the value of ε_a. The curves with constant error in the phase are similar to circumferences with center located along an axis $\Im\{k_0\mathbf{R_s}\} = -0.5$ and are tangent to $\Im\{k_0\mathbf{R_s}\}$ axis close to the origin. Again, as longer is the radius of these circumferences, smaller is the error ε_p. These results *motivated* the initial idea of introducing the general concept of a *complex distance* and the analysis made in [6], and summarized in **Part I**.

For a fixed value of $|k_0\mathbf{R_s}|$ the worse error in the absolute value and argument were found, Figure 5, leading to the values shown in Table 1.

3.2. Exponential term

The NHCW in (7), except for the constants, is constituted by two terms: the exponential term $e^{ik_0\mathbf{R_s}}$, and the square root term $1/(k_0\mathbf{R_s})$, both introducing amplitude and phase contributions. These two terms will be analyzed separately, and then will be considered together in order to find the field characteristics for the NHCW approximation. We will place a special emphasis on the exponential term (ET) because it constitutes the main contribution to the expression in (7) and, even if it is not a valid solution of the wave equation,

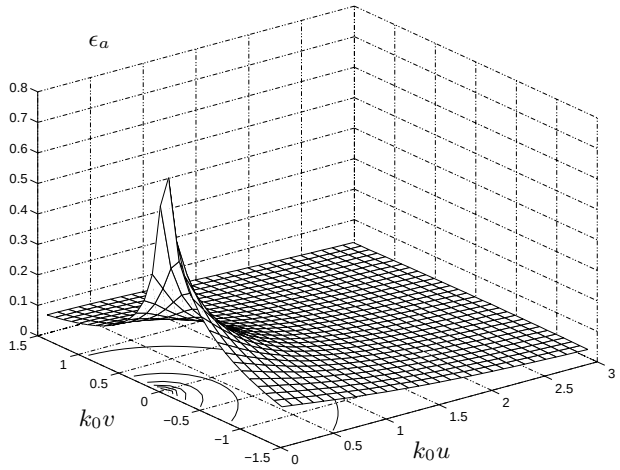

Figure 3. Error of the asymptotic approximation.

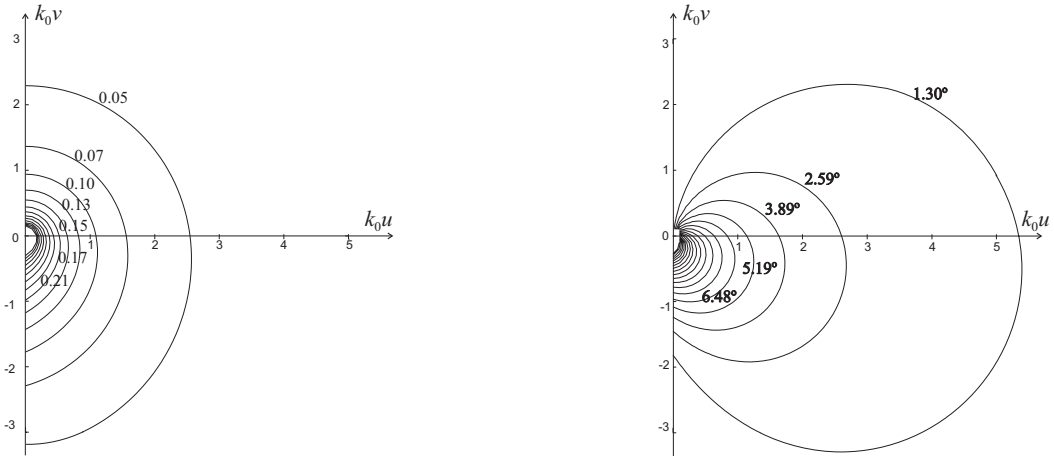

(a) (b)

Figure 4. Curves with constant (a) amplitude error, and (b) phase error.

Table 1. Error in the *CRC*

$\lvert k_0\mathbf{R_s}\rvert$	ε_{amax}	ε_{pmax}
2	8.8 %	3.6°
3	5.3 %	2.4°
4	3.7 %	1.8°
5	2.8 %	1.5°
7	2.0 %	1.1°
10	1.4 %	0.72°

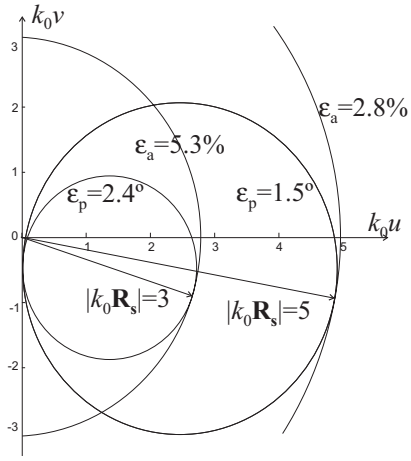

Figure 5. Error level in the asymptotic approximation assuming maximum values $|k_0\mathbf{R_s}| = 3$ and $|k_0\mathbf{R_s}| = 5$.

under some circumstances, it will directly represent the behavior of a NHCW. By calling $\mathbf{R_s} = u + iv$, the ET may be expressed as $e^{ik_0\mathbf{R_s}} = e^{-k_0v}e^{ik_0u}$.

3.2.1. Phase fronts

From $e^{ik_0\mathbf{R_s}} = e^{-k_0v}e^{ik_0u}$, curves with constant phase u, that is, straight lines in the complex $\mathbf{R_s}-$space (curve 4 in **Part I**), become confocal ellipses with focuses located at $z = \pm b$ in the real R_s-space,

$$\frac{\eta^2}{u^2 + b^2} + \frac{\xi^2}{u^2} = 1. \tag{10}$$

3.2.2. Phase paths

Curves with constant v (curve 3 in **Part I**) become confocal hyperbolas with focuses located at $\eta = \pm b$ in the real space, i.e., the orthogonal set of curves to those in (10),

$$\frac{\eta^2}{b^2 - v^2} - \frac{\xi^2}{v^2} = 1. \tag{11}$$

In this particular case, the phase paths are the same set of curves than the curves with constant amplitude. Both, curves in (10) and (11) are graphically depicted in Figure 6.

3.2.3. Equivalent beam width

We will introduce an equivalent beam width, an equivalent curvature center and a curvature radius, which will be useful for comparisons with the well-known Gaussian beam solution recalled in next section.

We will define the equivalent beam width, $\mathcal{W}_{eq}$, for the exponential term as the real η coordinate where the amplitude decays to $1/e$ from its maximum value. In the real space, the expressions are difficult to manage, but those expressions become simpler when their are formulated in the complex space. We will use the SCD and then, we will translate the results into the real space. The $\mathcal{W}_{eq}$ is defined by imposing the condition that the amplitude decays to $1/e$. From $k_0v = \frac{-k_0}{\sqrt{2}}\sqrt{\sqrt{(\xi^2 + \eta^2 - b^2)^2 + 4\xi^2b^2} - (\xi^2 + \eta^2 - b^2)}$,

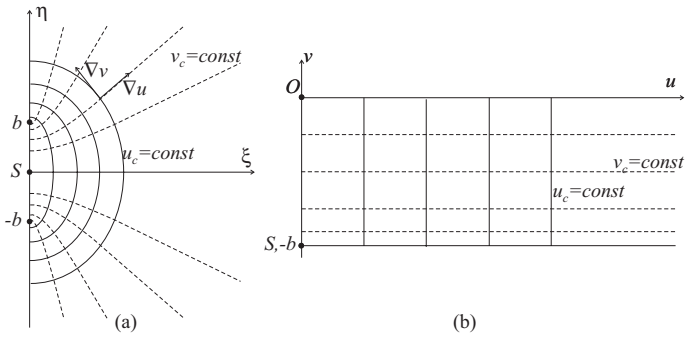

Figure 6. Curves with constant u and v. In the SCD (b), they are straight parallel lines to the axes, in the RPS (a), become ellipses and hyperbolas.

by making $\eta = 0$ it may be found straight forward that $k_0 v_0 = -k_0 b$, being v_0 the value of v when $\eta = 0$. From $e^{-k_0 v} = e^{-k_0 v_0 - 1}$ we get $-k_0 v = -k_0 v_0 - 1$, leading to

$$k_0 v_0 = -k_0 b + 1. \tag{12}$$

This simple expression in the complex space may be mapped into the real space, leading to a line parallel to the $k_0 v$ axis. The condition $k_0 b \geq 1$ must be imposed. If $k_0 b \leq 1$, $\mathcal{W}_{eq}$ makes no sense because the amplitude does not decay far away from the axis, in fact, when $k_0 b \to 0$ the NHCW becomes a cylindrical wave. The curve $k_0 v = -k_0 b + 1$ becomes,

$$\frac{\eta^2}{b^2 - \frac{(-k_0 b+1)^2}{k_0^2}} - \frac{\xi^2}{\frac{k_0^2}{(-k_0 b+1)^2}} = 1, \tag{13}$$

into the real space, which is an hyperbola with vertex at $\eta = \pm\sqrt{\frac{2k_0 b-1}{k_0^2}}$. The beam width shape is represented in Figure 7.

The Gaussian beam width is usually expressed in terms of the beam width at the origin $\mathcal{W}_0$. For the ET analyzed here, the value of $\mathcal{W}_{eq}$ when $(k_0 u = 0, k_0 v = -k_0 b + 1)$ will be called $\mathcal{W}_{eq,0}$, and will be $(\xi = 0, \eta = \pm\sqrt{\frac{2k_0 b-1}{k_0^2}}$ in the RPS. Thus, we can write $\mathcal{W}_{eq,0} = \sqrt{\frac{2k_0 b-1}{k_0^2}}$. By comparison with a Gaussian Beam where $\mathcal{W}_0 = \sqrt{2b/k_0}$, we can write the following relation,

$$\mathcal{W}_{eq,0} = \sqrt{\mathcal{W}_0^2 - 1}. \tag{14}$$

3.2.4. Equivalent curvature center

It was previously found that phase fronts are ellipses in the form $\frac{\eta^2}{u^2+b^2} + \frac{\xi^2}{u^2} = 1$. In Figure 8 the constant phase is parameterized by u_i. These ellipses may be also written as,

$$\begin{aligned} \xi &= u \cos t \\ \eta &= \sqrt{u^2 + b^2} \sin t, \qquad -\frac{\pi}{2} \leq t \leq \frac{\pi}{2}. \end{aligned} \tag{15}$$

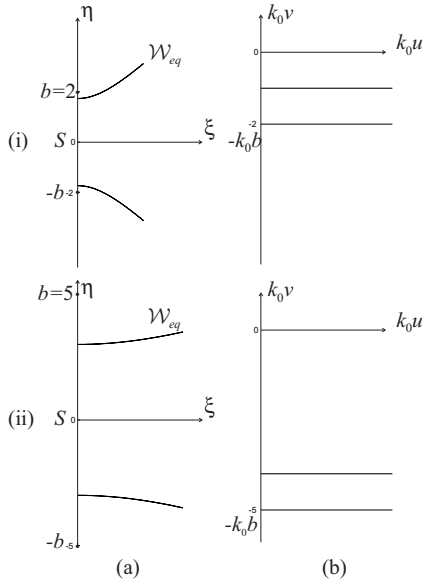

Figure 7. Equivalent beam width $\mathcal{W}_{eq}$ for the exponential term. Example (i) with $k_0 = 1,\ b = 2$, and (ii) with $k_0 = 1,\ b = 5$. Representation (a) in the RPS, and (b) in the SCD.

By choosing a fixed point $P_0 = (\xi_0, \eta_0)$ which belongs to a phase front given by u, we can find the tangent and the perpendicular line to that ellipse at the point P_0, Figure 8a. Considering two points separated a differential angle, Figure 8a, and doing the same procedure, the curvature center (ξ_c, η_c) may be found as the intersection of the two perpendicular lines, obtaining,

$$\begin{aligned} \xi_c &= -\frac{2u^2 + b^2}{u}\cos^3 t_0 \\ \eta_c &= \frac{\sin t_0(-(2u^2 + b^2)\cos^2 t_0 + b^2)}{\sqrt{u^2 + b^2}} \end{aligned} \tag{16}$$

It is possible to find a explicit equation $\eta_c(\xi_c)$ but the parametric form in (16) is more convenient to analyze the shape of this function, which is represented in Figure 8b.

3.2.5. Equivalent curvature radius

The curvature radius is defined as the distance between any point P_0 in the RPS and its curvature center, $\mathcal{R}_{eq} = \sqrt{(\xi_0 - \xi_c)^2 + (\eta_0 - \eta_c)^2}$. It is also represented in Figure 8.

3.3. Square root term

The second term constituting the NHCW field solution in (7) is the square root term $1/\sqrt{\mathbf{R_s}}$. introducing both, amplitude e^{β} and phase $e^{i\varphi}$ contributions, which may be written in terms of $\mathbf{R_s} = u + iv$ as,

$$e^{\beta} = \frac{1}{\sqrt[4]{u^2 + v^2}}, \tag{17}$$

$$\varphi = -\frac{1}{2}\arctan\left(\frac{v}{u}\right). \tag{18}$$

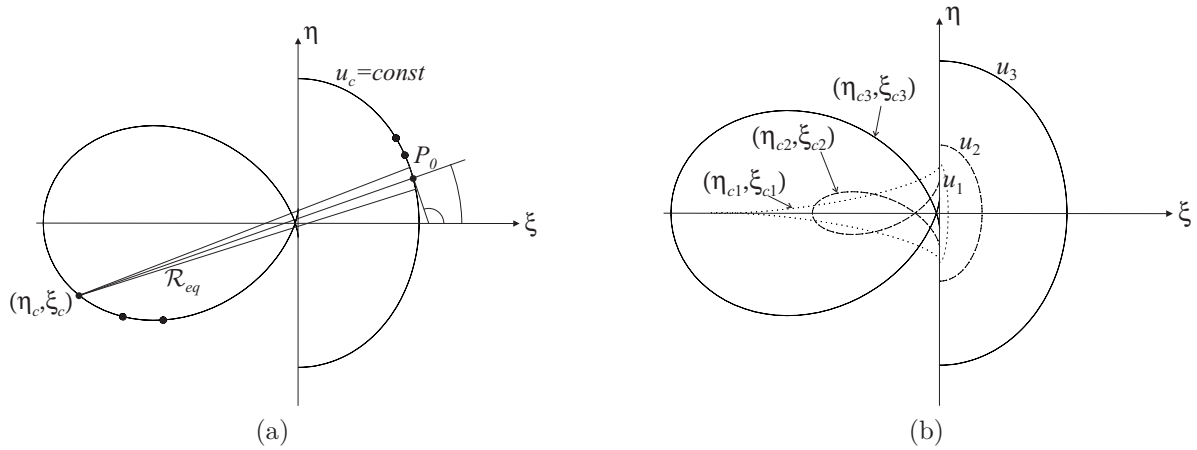

Figure 8. (a) The equivalent curvature center at an arbitrary point P_0. (b) Equivalent curvature center for different phase fronts u_i.

3.3.1. Constant amplitude curves

From (17), imposing the condition $u^2+v^2 = const$ in the SCD and applying the parametric relations between the SCD and the RPS developed in **Part I**, the curves with constant amplitude may be mapped into the RPS leading to bicuadratic lemniscatas,

$$\rho^4 - b^4 = (\xi^2 + \eta^2)^2 + 2b^2(\xi^2 - \eta^2). \tag{19}$$

This will be procedure to find most of the NHCW characteristics: systematically, they will be defined and obtained in the SCD, and then the results will be mapped into the RPS. The curves in (19) are also the limit of the Complex Radiation Condition, or validity range of (7), with ρ describing the error in the approximation, [6]. These sets of curves are plotted in Figure 9.

3.3.2. Phase fronts

From (18), and following the same procedure, the curves with constant phase become circumferences in the RPS with center located at $\eta = \frac{b}{2}\frac{1-m^2}{m}$ and with radius $b\sqrt{1+\frac{(1-m^2)^2}{4m^2}}$; both are parameterized in terms of the slope in the SCD, $m = -v/u$,

$$\eta^2 + x^2 + \xi b\frac{1-m^2}{m} - b^2 = 0. \tag{20}$$

These results are shown in Figure 9.

3.3.3. Phase paths

The phase paths may be found as the set of curves orthogonal to the phase fronts in (20). A way to obtain a perpendicular set of curves to a given one in the 2D real space reduces to the resolution of a first order differential equation, [7]. In this case, the orthogonal set of curves to the phase fronts are circumferences with center at $\eta = \lambda/2$ and radius $\sqrt{\frac{\lambda^2}{4} - b^2}$. These are expressed in terms of a parameter λ related to the phase value, $\lambda \geq 2b$,

$$\eta^2 + \xi^2 - \lambda\eta + b^2 = 0. \tag{21}$$

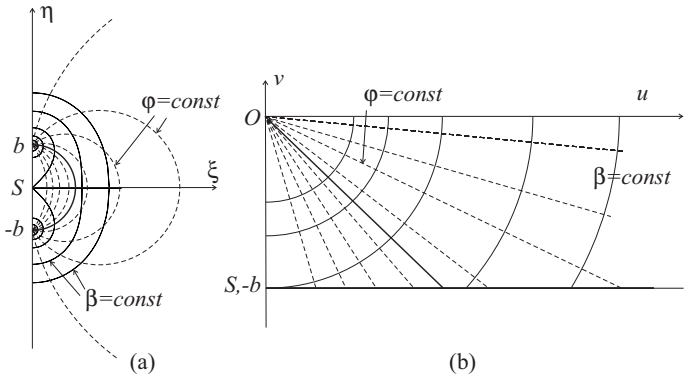

Figure 9. Curves with constants φ and β, (a) in the RPS, and (b) in the SCD.

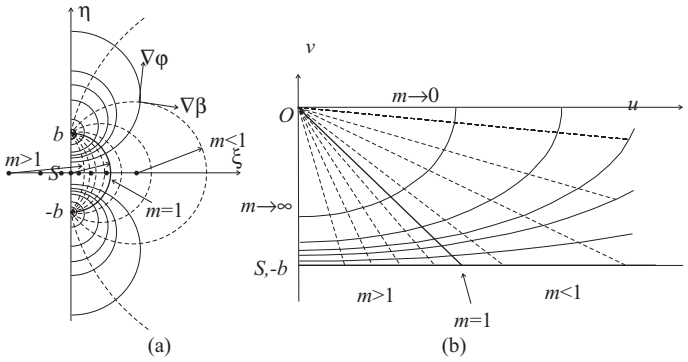

Figure 10. Phase fronts and phase paths for the square root term (a) in the RPS, and (b) in the SCD.

Both, the phase fronts and the phase paths for the square root term contribution are plotted in Figure 10. It is important to remark that the curves $\beta = const$ and $\varphi = const$ are *orthogonal sets in the SCD but not in the RPS*. Phase paths are located along $\nabla\varphi$ by definition, so, the curves $\varphi = const$ and $\nabla\varphi$ are orthogonal on the RPS and the curves $\beta = const$ and $\nabla\varphi$ are not orthogonal on the RPS.

Phase paths may also be found by using the auxiliary *Elliptical Coordinates Plane* (ECP) which is developed in Appendix II. The orthogonal condition may be mapped from the RPS into the ECP; all the expressions and the differential equation which must be solved are on the ECP simpler than those on the RPS. Curves $u/v = const$ may be mapped into the ECP leading to $\sin l_2/\mathrm{sh} l_1 = const$. By imposing the orthogonal condition in the ECP, the same solution plotted in Figure 10 was obtained.

3.4. Field parameters

The analysis of the inhomogeneous cylindrical waves requires both, the exponential and the square root terms. The phase paths, phase fronts and amplitude constant curves for the complete solution will be summarized in this section. By calling $C_a e^{\alpha_{C_p}}$ to the constant terms in (7), we can rewrite the Green's function,

$$G_f = C_a e^{\alpha_{C_p}} \frac{e^{ik_0 \mathbf{R_s}}}{\sqrt{\mathbf{R_s}}} = C_a e^{\alpha_{C_p}} e^{\beta - k_0 v} e^{i(k_0 u + \varphi)}. \tag{22}$$

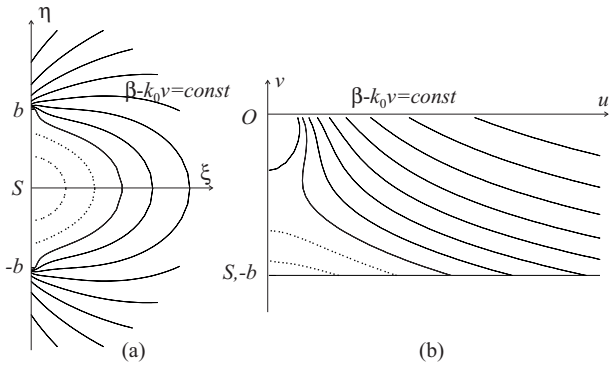

Figure 11. Curves of constant amplitude for an inhomogeneous cylindrical wave, (a) in the RPS, and (b) in the SCD.

3.4.1. Curves with constant amplitude

This curves are obtained by making $\beta - k_0 v = \lambda$,

$$-\frac{1}{4}\mathrm{Ln}(u^2 + v^2) - k_0 v = \lambda, \tag{23}$$

and are plotted in Figure 11b. It is only possible to obtain explicit expression in the space of real coordinates under certain approximations. By using the parametric expressions, the curves plotted in Figure 11a are obtained.

3.4.2. Phase fronts

The curves with constant phase are obtained by making $k_0 u + \varphi = const$, leading to,

$$k_0 u - \frac{1}{2}\tan^{-1}\frac{u}{v} = \lambda. \tag{24}$$

These curves are plotted in Figure 12b. From the parametric expressions we can see the behavior of these curves in the real space, Figure 12a.

3.4.3. Phase paths

From the orthogonal relations described in last sections, the goal is to find $\nabla k_0 u + \nabla\varphi = 0$ in the RPS, that is, the set of curves orthogonal to (24). Up to our knowledge, there is not an analytic solution to the resulting differential equation when it is formulated in the RPS, The problem was translated to the ECP and, even when the resulting differential equation expression is much simpler, we have still not found an analytic solution. The solution was found numerically by imposing the orthogonal condition in the auxiliary ECP, obtaining the result shown in Figure 12.

As a summary, the curves with constant amplitude, phase fronts and phase paths for the exponential term, the square root term and the inhomogeneous cylindrical wave are plotted in Figures 13, 14 and 15 showing the relation between all the spaces.

3.5. EP-NHCW: high frequency/far field approximation

The NHCW expression in (7) was used in previous development to get the curves in Figure 12, where the *CRC* limit is also plotted. The results in this figure and their comparison with the isolated exponential term

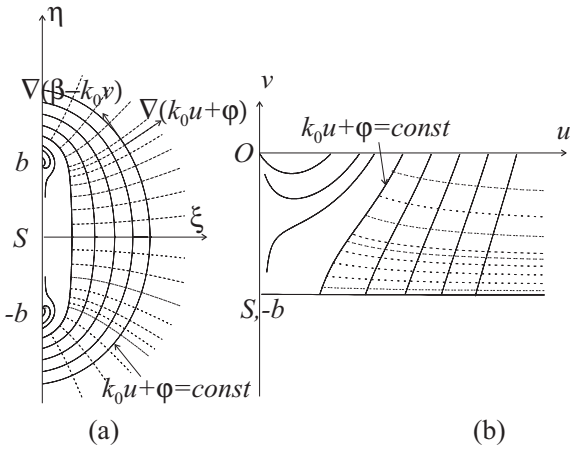

Figure 12. Phase fronts and phase paths for an inhomogeneous cylindrical wave, (a) in the RPS, and (b) in the SCD.

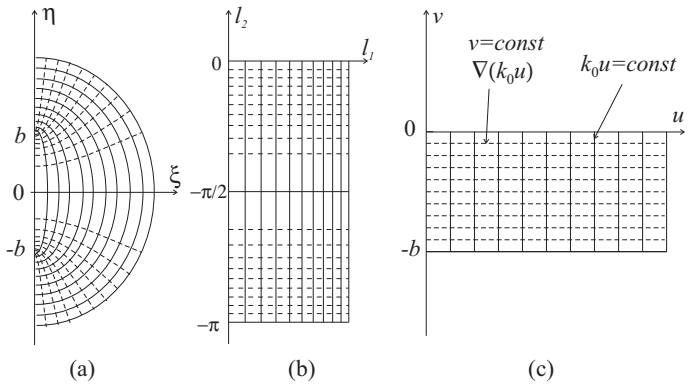

Figure 13. Curves of constant amplitude, phase fronts and phase paths for the exponential term an inhomogeneous cylindrical wave. Representation (a) in the RPS; (b) in the ECP, and (c) in the SCD.

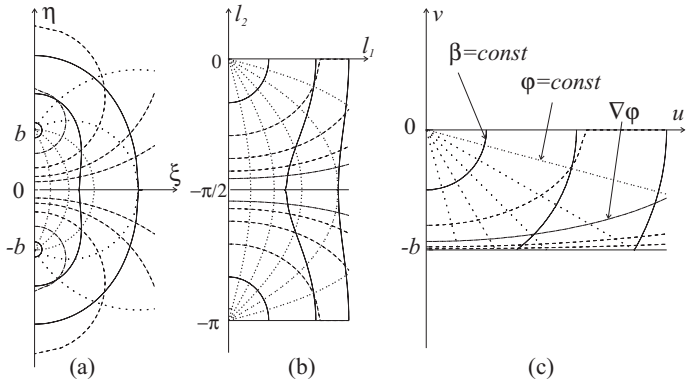

Figure 14. Curves of constant amplitude, phase fronts and phase paths for the square root term. Representation (a) in the RPS; (b) in the ECP, and (c) in the SCD.

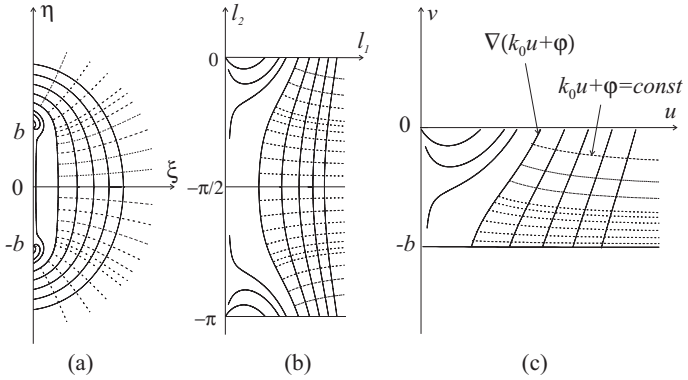

Figure 15. Phase fronts and phase paths for an inhomogeneous cylindrical wave. Representation (a) in the RPS; (b) in the ECP, and (c) in the SCD. Curves of constant amplitude have been omitted for simplicity.

shown in Figure 6 suggest the following approximation: by neglecting φ in NHCW the phase would reduce to the exponential term phase contribution and the phase fronts and paths would be those given by (10) and (11).

In *HF-FF* regime (notice that k_0 is related to the frequency and u is related to the spatial distance), phase can be approximated by neglecting term φ,

$$k_0u + \varphi \sim k_0u, \tag{25}$$

and the filed solution will have elliptic phase fronts, Figure 6, are valid in this region, Figure 16.

Let us call $\varepsilon = 1/\rho_{HN}$ to the relative error in this approximation,

$$\frac{k_0u}{\varphi} = \rho_{HN}, \quad \rho_{HN} \geq 1, \tag{26}$$

which may be also written as,

$$v \leq -u \tan \frac{2k_0u}{\rho_{HN}}. \tag{27}$$

The curves with constant $k_0\varepsilon$ are represented in Figure 16. For a fixed point, ε depends on k_0. As k_0 increases, the criterion with σ may be more relaxed keeping the same relative error.

Under these circumstances, the field solution will be an *Elliptical Phase-Non Homogeneous Cylindrical Wave* EP-NHCW, that may be written in the form,

$$G_f(k_0\mathbf{R_s}) \sim \frac{e^{i\frac{\pi}{4}}}{2\sqrt{2\pi}} \frac{e^{-k_0v}}{\sqrt{k_0(u^2+v^2)}} e^{ik_0u}. \tag{28}$$

It is important to realize that the high frequency approximation in (25) makes sense only in the complex radiation condition validity region because it was obtained from the NHCW expression in (7). This fact may be checked with next example: for a point $P = (\xi = 0, \eta = b - \varepsilon)$, with ε arbitrarily small, when k_0 is large enough, point P may be in the region where condition (25) is valid, but phase in P is not given by k_0u. *HF-FFC* cannot be extended up to the source location. The validity range may be only extended, once k_0 is fixed, when the error value is relaxed.

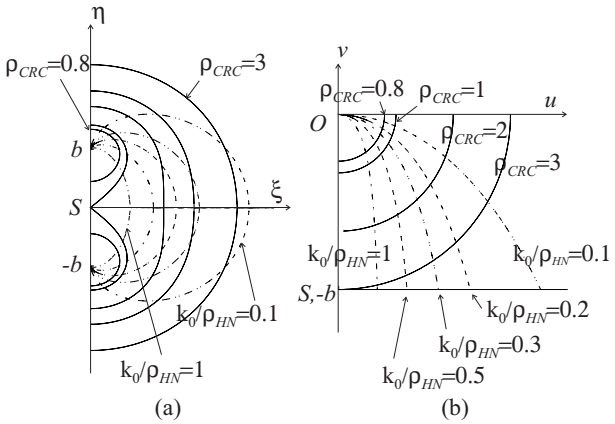

Figure 16. Validity region of *CRC* and *HF-FFC* (a) in the RPS, and (b) in the SCD.

4. Gaussian Beams

4.1. Paraxial condition

Once the *CRC* is assumed, by applying the *Paraxial Condition* (*PC*) to (7), the well-known *Gaussian Beam* (GB) solution is obtained. The *PC* may be defined as,

$$\eta^2 \leq \xi^2 + b^2. \tag{29}$$

The parameter ρ_{PC} will be used to parameterize the approximation and the *PC* will be written as,

$$\eta^2 \leq \frac{\xi^2 + b^2}{\rho_{PC}^2}, \quad \rho_{PC} \geq 1. \tag{30}$$

This curve defines the *PC* and will be carefully analyzed later in this section.

Assuming the *PC*, the complex distance may be approximated by the first terms of its Taylor's series leading to,

$$\begin{aligned} |\vec{r} - \vec{\mathbf{r}}_\mathbf{s}| &= \sqrt{(\xi - ib)^2 + \eta^2} \\ &\simeq \xi - ib + \frac{\eta^2}{2(\xi - ib)} \\ &= \xi - ib + \frac{\eta^2(\xi + ib)}{2(\xi^2 + b^2)} \\ &= \xi + \frac{\xi\eta^2}{2b^2(\frac{\xi^2}{b^2} + 1)} - i\left(b - \frac{\eta^2}{2b(\frac{\xi^2}{b^2} + 1)}\right) \end{aligned} \tag{31}$$

$$\begin{aligned} ik_0|\vec{r} - \vec{\mathbf{r}}_\mathbf{s}| &= ik_0\left(\xi + \frac{\eta^2}{\frac{2b^2}{\xi}(1 + \frac{\xi^2}{b^2})}\right) + k_0 b - \frac{\eta^2}{\frac{2b}{k_0}(1 + \frac{\xi^2}{b^2})} \\ &= ik_0(\xi + \frac{\eta^2}{2\mathcal{R}(\xi)}) + k_0 b - \frac{\eta^2}{\mathcal{W}^2(\xi)}, \end{aligned} \tag{32}$$

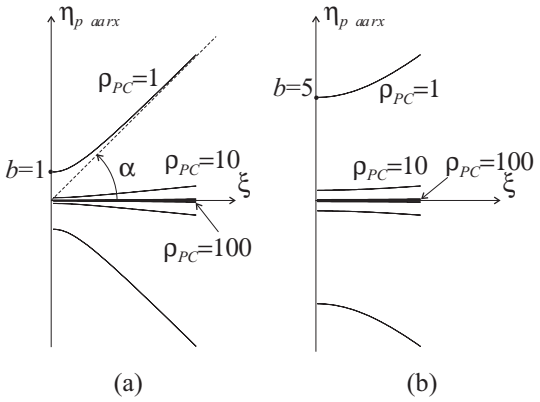

Figure 17. Limit of the *PC* validity range for $\rho_{PC} = 1, 10, 100$; (a) $b = 1$, and (b) $b = 5$.

where,

$$\mathcal{W}^2(\xi) = \frac{2b}{k_0}\left(1 + \frac{\xi^2}{b^2}\right), \tag{33}$$

$$\mathcal{R}(\xi) = \frac{b^2}{\xi}\left(1 + \frac{\xi^2}{b^2}\right) = \frac{b^2 + \xi^2}{\xi}. \tag{34}$$

$\mathcal{W}(\xi)$ in (33) defines the beam width in such a way that $\mathcal{W}(\xi) = \eta_{\mathcal{W}}$, being $\eta_{\mathcal{W}}$ the coordinate where the amplitude decays to $1/e$. When $\xi = 0$, $\mathcal{W}_0^2 = 2b/k_0$ and the beam width at the beginning of the beam will be given by,

$$\mathcal{W}_0 = \sqrt{\frac{2b}{k_0}}. \tag{35}$$

The following relation may be written in terms of $\mathcal{W}_0$,

$$\eta_{\mathcal{W}} = \mathcal{W}_0\sqrt{1 + \frac{\xi^2}{b^2}}. \tag{36}$$

$\mathcal{R}(\xi)$ in (34) defines the curvature radius of the phase front. As the beam propagates along ξ-direction, $\mathcal{R}(\xi)$ changes, as described in section 4.2.

Under these circumstances, using the approximation in (31) for the phase term, and approximating $|\vec{r} - \vec{\mathbf{r}}_{\mathbf{s}}| \sim \xi - ib$ for the amplitude term, both in (7), we find the usual GB expression,

$$G_f \sim \frac{e^{i\frac{\pi}{4}}}{2\sqrt{2\pi}} \frac{e^{k_0 b}}{\sqrt{k_0(\xi - ib)}} e^{\frac{-\eta^2}{\mathcal{W}^2(\xi)}} e^{ik_0\left(\xi + \frac{\eta^2}{2\mathcal{R}(\xi)}\right)}. \tag{37}$$

4.1.1. Paraxial condition parameterization

The *PC* validity will be analyzed in terms of the parameter ρ_{PC} defined in (30). This curve is an hyperbola in the RPS with an asymptote defined by an angle α with respect to the beam axis. ($\tan\alpha = \lim_{\xi\to\infty} d\eta/d\xi = 1/\rho_{PC}$.) Some examples are shown in Figure 17.

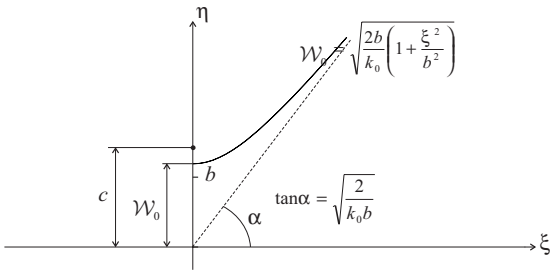

Figure 18. Parameters defining the beam width of a Gaussian Beam. Example with normalized values $k_0 = 1$ and $b = 1$.

Given a ρ_{PC} value, the beam width must be included inside the validity region in (30). From (33), we can see that the beam width is defined by,

$$\eta^2 = \frac{2b}{k_0}\left(1 + \frac{\xi^2}{b^2}\right) = \frac{2b}{k_0} + \frac{2}{k_0 b}\xi^2, \tag{38}$$

$$\frac{\eta^2}{2b/k_0} - \frac{\xi^2}{b^2} = 1. \tag{39}$$

The result in (39) is an hyperbola with vertex at $\mathcal{W}_0 = \sqrt{2b/k_0}$, confocal parameter $c = \sqrt{\mathcal{W}_0^2 + b^2}$ and eccentricity $e = c/\rho_{PC} = \sqrt{1 + k_0 b/2}$, refer to Figure 18. The hyperbola asymptotes have a slope given by,

$$\tan\alpha = \lim_{\xi\to\infty}\frac{d\eta}{d\xi} = \pm\sqrt{\frac{2}{k_0 b}}. \tag{40}$$

The limit of the paraxial region will be located within the beam width when

$$\eta_{\mathcal{W}} = \sqrt{\frac{2b}{k_0}\left(1 + \frac{\xi^2}{b^2}\right)} < \eta_{parax} = \frac{\sqrt{\xi^2 + b^2}}{\rho_{PC}}, \tag{41}$$

leading to the following condition

$$k_0 > \frac{2\rho_{PC}^2}{b}. \tag{42}$$

This means that a value of b may be found in such a way that the paraxial condition holds with any desired ρ_{PC}, if the frequency is large enough. Examples of this condition are shown in Figures 19 and 20 and in Table 2. The frequency values were obtained assuming propagation in vacuum. These values are also represented in Figure 21.

It is important to distinguish between the paraxial limit described by (30) and the fact of keeping the beam width within the paraxial region, as described in (42). Let us illustrate the difference with an example. On choosing $\rho_{CRC} = 5$, $b = 1$ and $\rho_{PC} = 10$. Condition in (42) will hold if $k_0 \geq 200$. In the case with $k_0 = 5$, condition in (42) does not hold. The values of the NHCW and GB Green's functions are compared in Figure 22 when $\xi = 5$. Closed to the ξ axis, condition in (30) holds and both functions fit each other. In Figure 23 the same functions are represented choosing the same values $\rho_{CRC} = 5$, $b = 1$ and $\rho_{PC} = 10$, but now with $k_0 \geq 200$ which verifies (42). Now, both functions fit everywhere. The GB approximation may be now used inside and outside the paraxial region.

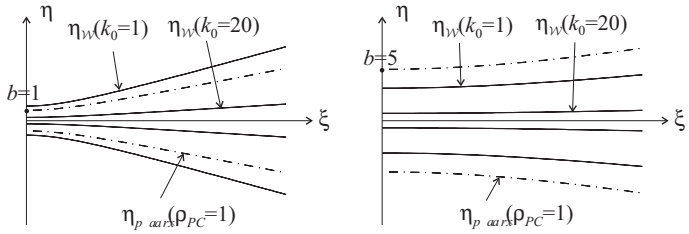

Figure 19. Paraxial region with $b = 1$ and $b = 5$, fixing $\rho_{PC} = 1$.

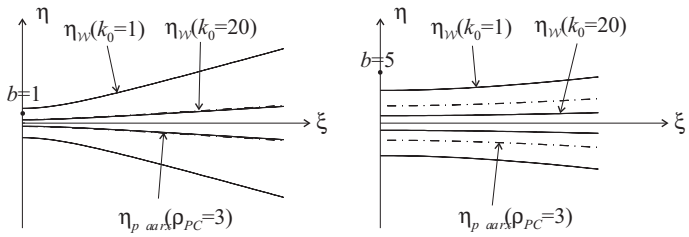

Figure 20. Paraxial region with $b = 1$ and $b = 5$, with $\rho_{PC} = 3$.

Table 2. Wavenumber and frequency to keep the GB inside the paraxial region.

$\rho_{PC} = 1$

b	$k_0(rad/m)$	$f_0(GHz)$
0.1	20	0.955
0.5	4	0.191
1	2	0.096
5	0.4	0.019

$\rho_{PC} = 10$

b	$k_0(rad/m)$	$f_0(GHz)$
0.1	2000	95.49
0.5	400	19.10
1	200	9.55
5	40	1.91

$\rho_{PC} = 100$

b	$k_0(rad/m)$	$f_0(GHz)$
0.1	200000	9549.29
0.5	40000	1909.86
1	20000	954.93
5	4000	190.99

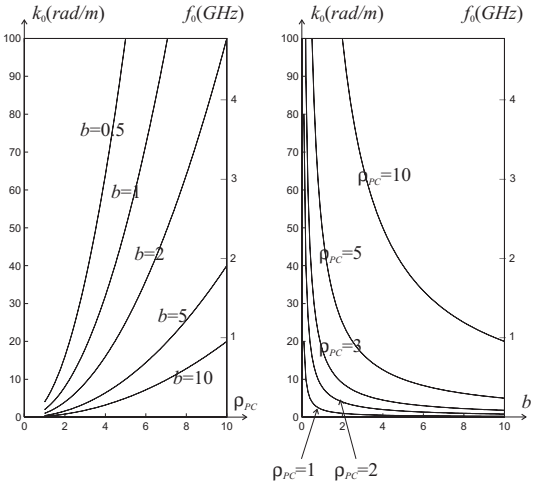

Figure 21. Wavenumber and frequency to keep the beam inside the paraxial region for different values of b and ρ_{PC}.

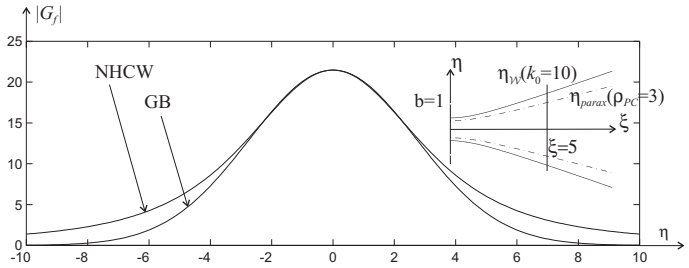

Figure 22. Green's function amplitude on a straight line $\xi = 0.5$, with $b = 1$ and $k_0 = 10$.

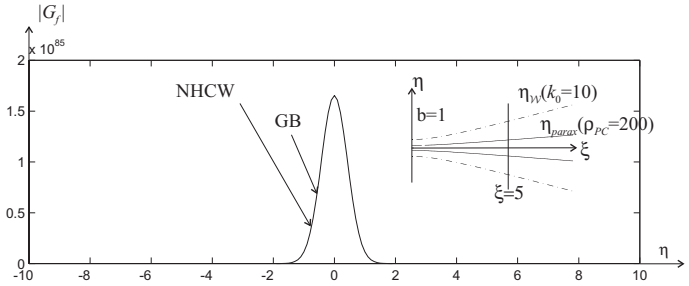

Figure 23. Green's function amplitude on a straight line $\xi = 0.5$, with $b = 1$ and $k_0 = 200$.

4.1.2. Paraxial condition validation

An alternative parameterization of the PC may be found by taking the fourth order term in the Taylor's Series used previously to approximate $\mathbf{R_s} = \sqrt{(\xi - ib)^2 + \eta^2}$ when $\eta^2 \ll |\xi - ib|^2$,

$$\sqrt{(\xi - ib)^2 + \eta^2} \sim (\xi - ib) + \frac{\eta^2}{2(\xi - ib)} - \frac{\eta^4}{8(\xi - ib)^3}. \tag{43}$$

The first two terms correspond to the paraxial approximation, while the third term, which is a fourth order term may be used to define a new parameter ρ'_{PC},

$$\rho'_{PC} = \frac{|\xi - ib| + \frac{\eta^2}{2|\xi - ib|}}{\frac{\eta^4}{8|\xi - ib|^3}}, \quad \rho'_{PC} \geq 1. \tag{44}$$

After some algebra,

$$\rho'_{PC} = 8\frac{|\xi - ib|^4}{\eta^4} + 4\frac{|\xi - ib|^2}{\eta^2}. \tag{45}$$

By comparison with ρ_{PC} in (30) we find that,

$$\rho'_{PC} = 8\rho_{PC}^2 + 4\rho_{PC}, \tag{46}$$

and the PC may be parameterized in terms of either ρ_{PC} in (30)or ρ'_{PC} related to the fourth order term in Taylor's series.

4.2. Field parameters

GB's parameters may be analyzed in the Real Propagation Space. The usual results are analyzed in detail in [2] and may be briefly summarized as:

- Amplitude variation

  Cylindrical term, $1/\sqrt{\xi^2 + b^2}$.

  Gaussian term, $\exp(-\eta^2/\mathcal{W}^2(\xi))$.

  Beam width analysis, $\mathcal{W}^2(\xi) = \frac{2b}{k_0}\left(1 + \frac{\xi^2}{b^2}\right)$.

  Curves with constant amplitude.

- Phase variation

  $k_0\xi$ term.

  $\phi = \tan^{-1}(b/\xi)/2$ term.

  $\eta^2/2\mathcal{R}$ term.

  Curvature radius $\mathcal{R}(\xi) = \frac{b^2}{\xi}\left(1 + \frac{\xi^2}{b^2}\right)$ and center.

  Phase fronts.
  Phase paths.

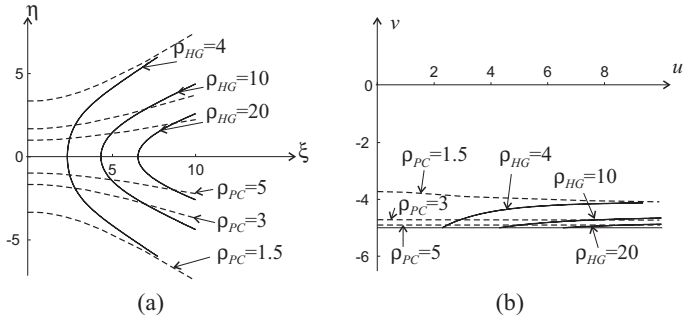

Figure 24. *HF-FFC* for GB with $\rho_{HG} = 4.5, 18, 50$ and *PC* with $\rho_{PC} = 1.5, 3, 5$.

4.3. PP-GB: high frequency/far field approximation for GB's

This section runs parallel to section 3.5 but applied to GB's instead of NHCW's. The idea is to parameterize the condition which allows to approximate the phase of a GB by its main contribution, leading to a plane phase front. This approximation is widely used in works involving GB's.

From (37), the Green's function may be rewritten as,

$$G_f = \frac{e^{i\frac{\pi}{4}}}{2\sqrt{2\pi}} \frac{e^{k_0 b}}{\sqrt{k_0}} \frac{e^{\frac{-\eta^2}{\mathcal{W}^2(\xi)}}}{\sqrt[4]{\xi^2+b^2}} e^{ik_0\left(\xi+\frac{\eta^2}{2\mathcal{R}(\xi)}\right)+i\frac{1}{2}\tan^{-1}\frac{b}{\xi}}. \tag{47}$$

In *HF-FF* regime, the GB phase in (47), except for the constants, may be approximated by a plane phase coming from the most significant term,

$$k_0\xi + k_0\frac{\eta^2}{2\mathcal{R}(\xi)} + \frac{1}{2}\tan^{-1}\frac{b}{\xi} \sim k_0\xi, \tag{48}$$

leading to the PP-GB solution,

$$G_f \sim \frac{e^{i\frac{\pi}{4}}}{2\sqrt{2\pi}} \frac{e^{k_0 b}}{\sqrt{k_0}} \frac{e^{\frac{-\eta^2}{\mathcal{W}^2(\xi)}}}{\sqrt[4]{\xi^2+b^2}} e^{ik_0\xi}. \tag{49}$$

It must be noticed that *PC* must be necessary assumed. If not, term $\eta^2/2\mathcal{R}$ cannot be neglected; in fact, this term makes no sense if *PC* is not assumed.

Let us call ε, $(\varepsilon \leq 1)$ to the non-dimensional relative error,

$$\varepsilon = \frac{k_0\frac{\eta^2}{2\mathcal{R}(\xi)} + \frac{1}{2}\tan^{-1}\frac{b}{\xi}}{k_0\xi}, \tag{50}$$

which may be parameterized in terms of

$$\rho_{HG} = \frac{1}{\varepsilon}, \quad \rho_{HG} \geq 1. \tag{51}$$

The curves with constant error ε are plotted in Figure 24.

From the real analysis of the GB characteristics it may be found that $\phi = \tan^{-1}(b/\xi)/2$ contribution may be neglected when $\xi \gg 0$, specially if $k_0 \gg 1$. With this assumption, we could approximate,

$$\varepsilon \sim \frac{\frac{\eta^2}{2\mathcal{R}(\xi,b)}}{\xi} = \frac{\eta^2}{2(\xi^2+b^2)}, \tag{52}$$

or,

$$\rho_{HG} \sim \frac{2(\xi^2 + b^2)}{\eta^2}. \tag{53}$$

By comparison with the *PC*, $\eta^2 = (\xi^2 + b^2)/\rho_{PC}^2$, it is found that the error in the plane phase approximation for GB is related to the *PC* itself,

$$\rho_{HG} = 2\rho_{PC}^2. \tag{54}$$

As a conclusion, as long as the *PC* is good enough, the PP-GB may be assumed straight ahead. The approximation in (52) is identical to the *PC*. The comparison with the first definition of ε in (50) is shown in Figure 24.

5. Conclusions

From the results presented in this paper, some important conclusions may be found. In first place, let us recall that a more general solution for the 2D radiation problem has been obtained. This general complex solution (complex beams) includes a set of particular solutions obtained when applying different approximations, some of them very common in the specialized literature. The ranges of validity of this approximations, as well as other important physical parameterizations such as the amplitude and phase paths, phase fronts, energy paths, etc. may be analyzed in a clean way in the spaces of complex distances and angles, thus generating a set of important mappings that may be classified as done in **Part I**. These mappings, and their corresponding translation into the real space, may be generalized and used as *reference curves* for the application of this methodology to the particular problem of scattering under complex beams incidence, as well as the complete analysis (radiation and scattering) of other wave problems (for instance, those concerning evanescent plane waves and/or surface waves, as previously mentioned), providing a good insight of the kind of solutions to appear for any case, their particular behavior in the real space, and the physical interpretation of their behavior.

From the practical point of view, the 2D rigorous complex point source Green's function provides a frequency-independent formulation, and not only under high-frequency asymptotic approximation. This exact solution, and the complex analysis associated to it thus become a reference standard for the analysis and comparison of other practical and very important solutions obtained under certain approximations.

It is important to emphasize in our particular problem that the exact complex beam solution presents limitations for analytical developments such as integration and, from the numerical point of view, presents some difficulties to be evaluated, specially for large arguments. These two considerations make necessary to apply the asymptotic approximation, and study the different ranges of validity for any solution.

In our specific problem, the NHCW, which might be identified with a pseudo-Gaussian profile beam due to its amplitude behavior, has been carefully analyzed by using the SCD: systematically, the SCD was used to perform the calculations and to obtain some results, which were lately translated and interpreted into the RPS. All these calculations included amplitude and phase information simultaneously. In fact, both, the exponential and the square root terms include these two contributions.

In the GB solution, the complex phase may be analytically separated in the amplitude and phase terms leading to a real variable expression. This allows to simplify the study of the field solution with a conventional real variable analysis. The GB solution is valid not only in the paraxial region, but may be also extended into the whole RPS.

From the practical point of view, the methodology presented in these two papers, allows to simplify the formulation. All the expressions become shorter and simpler in terms of the SCD coordinates. Also, it is possible to define and obtain parameters such as the equivalent beam width and equivalent curvature center for the ET, which allow straight ahead comparisons with the GB solution. This was made at the same time that all the approximations were parameterized. On the other hand, all validity ranges and domains for the mentioned approximations have been parameterized in terms of quantitative non-dimensional parameters.

Also, the complex point source Green's function and the methodology presented here confirms the fact of the predominant exponential term effect utilized previously in the *Evanescent Wave Tracking*, [8].

Finally, this study constitute the basis to the analysis scattering problems under complex beams incidence, currently under preparation. Some initial results may be found in [2, 9]. These problems may be analyzed by a new method in the complex spatial domain, including the asymptotic evaluation of the radiation integral. The incident non-homogeneous phase field, the Green function of the problem and the scattered fields, may be formulated in terms of the complex variable arising from the complex-point-source concept. That kind of problems may be analyzed in terms of complex distances, complex angles and complex rays and then interpreted in the real propagation space.

Appendix I. Computation of Hankel Function

To obtain any *'exact'* value of the Hankel function, it is necessary to use some computation. A program provides a concrete value of the function by making internal calculations which include series expansions in such a way that, in practice, it provides a more or less accurate approximation. Thus, the first point will be the analysis of the accuracy of the Hankel function, so-called exact values.

Let us obtain the Hankel function values $H_0^{(1)}(\mathbf{z}) = J_0(\mathbf{z}) + iY_0(\mathbf{z})$ with $J_0(\mathbf{z})$ and $Y_0(\mathbf{z})$, these two obtained with the ascendent series that may be found in [5],

$$J_0(\mathbf{z}) = 1 - \frac{\frac{1}{4}\mathbf{z}^2}{(1!)^2} + \frac{\left(\frac{1}{4}\mathbf{z}^2\right)^2}{(2!)^2} - \frac{\left(\frac{1}{4}\mathbf{z}^2\right)^3}{(3!)^2} + \ldots \quad , \tag{55}$$

$$\begin{aligned} Y_0(\mathbf{z}) = {} & \frac{2}{\pi}\left\{ ln(\frac{1}{2}\mathbf{z}) + \gamma \right\} J_0(\mathbf{z}) + \\ & \frac{2}{\pi}\left\{ \frac{\frac{1}{4}\mathbf{z}^2}{(1!)^2} - (1+\frac{1}{2})\frac{\left(\frac{1}{4}\mathbf{z}^2\right)^2}{(2!)^2} + (1+\frac{1}{2}+\frac{1}{3})\frac{\left(\frac{1}{4}\mathbf{z}^2\right)^3}{(3!)^2} - \ldots \right\}, \end{aligned} \tag{56}$$

where γ is the Euler constant. For each $\mathbf{z}$, a number of terms n should be taken in the series in such a way that the n-term $\frac{\mathbf{z}^{2n}}{4^n(n!)^2} \ll J_0(\mathbf{z})$, that is, in such a way that $(n!)^2$ becomes larger enough than $\mathbf{z}^{2n}$ compared to $J_0(\mathbf{z})$ value.

The accuracy only depends on the absolute value of $\mathbf{z}$, $|\mathbf{z}|$, and do not depend on its argument. Once a desired value of ε is fixed, for instance, $\varepsilon = 1\%$, the validity condition will be in the form $\frac{\text{term } n}{J_0(\mathbf{z},n)} \leq \varepsilon$. In Table 3, the values of $J_0(|\mathbf{z}|, n)$ with $|\mathbf{z}| = 3$ are compared with the value of the cutting term n.

With this guideline, the number of terms which are necessary to find the value of the Hankel function of complex arguments with a fixed error is obtained. It was found that there is a linear relation between these two parameters and they may be related by the straight line $n = \frac{3}{2}|\mathbf{z}| + 1$. We will establish the

Table 3. Number of terms for the exact solution computation

n	Term n	$J_0(3,n)$
0	1	1
1	-2.25	-1.25
2	1.26	0.01
3	-0.31	-0.30
4	0.04	-0.25
5	-0.004	-0.2603

criterion $n_{min} = \frac{3}{2}|\mathbf{z}_{max}| + 2$. It has been checked that this rule is valid in the half plane $\Re\{\mathbf{z}\} > 0$ until $|\mathbf{z}| = 15$. It makes no sense to consider higher values of $|\mathbf{z}|$ because the asymptotic approximation will be good enough when $|\mathbf{z}| \geq 15$. Under these conditions, we will assume that the computed values of the Hankel function are a good approximation to (1).

Appendix II. Auxiliary Transformations

The conformal mapping properties guarantee that two regular paths in an initial plane are mapped by an analytical function into two new paths keeping the same angle between the paths, [10]. For instance, this is the case of the transformation between $\mathbf{R}^2$ and $\mathbf{R}$.

From the definition of the complex distance, it is obvious than the mapping between the RPS and the SCD is not a conformal mapping, (neither between $\mathbf{R}^2$ and the RPS nor between $\mathbf{R}$ and the RPS). For this reason, the results of the complex analysis cannot be applied to these transformations. Thus, the following general rules must be kept in mind for the analysis of the phase fronts and phase paths of the NHCW:

- Resolution in the RPS: the phase paths are the set of curves orthogonal to the phase fronts. This orthogonal condition may be imposed in the RPS but the resulting differential equation is in general complicated.
- Resolution in the SCD: the orthogonal condition does not hold when the problem is mapped into the SCD; a translation or interpretation of the orthogonal condition into the SCD would be necessary in order to solve the problem in the SCD.
- Auxiliary transformations: the following coordinate system has been chosen in order to simplify the problem.

AII.1. Elliptical coordinates plane

The relation between the SCD and the RPS may be decomposed into two steps: (i) From the SCD into an auxiliary plane which will be called elliptical coordinates plane (ECP): (l_1, l_2) in such a way that the relationship between the RPS and the ECP is a change from rectangular into elliptical coordinates, [11],

$$\begin{aligned} l_1 &= \operatorname{ash}\frac{u}{b}, \\ l_2 &= \begin{cases} \operatorname{asin}\frac{v}{b}, & -\pi/2 \leq l_2 \leq 0 \\ -\pi + \operatorname{asin}\frac{v}{b}, & -\pi \leq l_2 \leq -\pi/2 \end{cases} \end{aligned} \tag{57}$$

and (ii) from the ECP to the RPS in the following way,

$$\begin{aligned} x &= -b\mathrm{sh}l_1 \sin l_2, \\ y &= b\mathrm{ch}l_1 \cos l_2. \end{aligned} \tag{58}$$

From the SCD into the ECP, the orthogonal condition between any two paths is not kept after the transformation, except for straight lines parallel to the axes. From the RPS into the ECP it may be found that $\nabla\psi = \frac{1}{h_{l_1}}\psi_{l_1}\hat{l_1} + \frac{1}{h_{l_2}}\psi_{l_2}\hat{l_2}$. As long as the metric $h_{l_1} = h_{l_2}$, the gradient in one plane is modified in its value but not in its direction with respect to the other one. We can conclude than the orthogonal condition in the RPS maps into an orthogonal condition in the ECP.

AII.2.Parabolic coordinates plane

The representation in the two planes $\mathbf{R}^2$ and the RPS corresponds with a change between rectangular and parabolic coordinates,

$$\begin{aligned} z_1 &= \frac{1}{\sqrt{2}}(u^2 - v^2), \\ z_2 &= \sqrt{2}uv. \end{aligned} \tag{59}$$

The orthogonal condition holds from one plane to the other, the same as with the elliptical coordinates. This fits with the result from the complex variable analysis and the conformal mapping condition.

Acknowledgments

To Prof. Carlos Dehesa Martínez for his interesting and stimulating discussions and ideas regarding this paper. Some of the studies presented in this paper were supported by the Spanish CICYT under grant PB97-0487.

References

[1] L. Felsen, *Complex-Source-Point Solutions of the Field Equations and their Relation to the Propagation and Scattering of Gaussian Beams.* Istituto Nazionale di Alta Matematica, Symposia Mathematica, Volume XVIII Bologna, 1976.

[2] M. González Morales, *Espacios Complejos. Aplicación a Problemas de Radiación y Dispersión Electromagnética de Haces.* Ph. Dissertation. Universidad de Valladolid, 2001.

[3] L. Felsen, *Complex Rays.* Philips Res. Repts 30, pp. 187-195, 1975.

[4] E. Heyman and L. Felsen, *Gaussian beam and pulsed-beam dynamics: complex-source and complex-spectrum formulations within and beyond paraxial asymptotics.* J. Opt. Soc. Am. A, Vol. 18, No. 7, pp. 1588-1611, 2001.

[5] M. Abramovitz and I. Stegun, *Handbook of Mathematical Functions.* Dover Publications, Inc. NY, 1970.

[6] E. Gago-Ribas, M. González Morales, and C. Dehesa Martínez, *Analytical Parametrization of a 2D Real Propagation Space in Terms of Complex Electromagnetic Beams.* Special Issue on Electromagnetic Theory-Scattering and Diffraction, IEICE Transactions on Electronics, Vol. E80-C, No.11, pp. 1434-1439, Japan, November 1997.

[7] F. Marcellán, L. Casasús, and A. Zazo, *Ecuaciones Diferenciales. Problemas Lineales y Aplicaciones.* McGraw-Hill, Madrid, 1990.

[8] P. Einziger and L. Felsen, *Evanescent Waves and Complex Rays.* IEEE Trans. on Ant. and Prop., Vol. 30, No. 4, pp. 594-604, July 1982.

[9] M. González Morales and E. Gago-Ribas, *On the Application of the Analytical Continuation to EM Fields.* The Fifth International Symposium on Antennas, Propagation ans EM Theory, ISAPE'2000, pp. 61-64. China, August 2000.

[10] A. Sveshnikov and A. Tikhonov, *The Theory of Functions of a Complex Variable.* MIR Publishers, Moscow, 1978.

[11] J. Stratton, *Electromagnetic Theory.* McGraw-Hill, New York, 1941.